# Van der Waals Heterostructured MOF-on-MOF Thin Films: Cascading Functionality to Realize Advanced Chemiresistive Sensing

*Ming-Shui Yao[+], Jing-Wei Xiu[+], Qing-Qing Huang, Wen-Hua Li, Wei-Wei Wu, Ai-Qian Wu, Lin-An Cao, Wei-Hua Deng, Guan-E Wang, and Gang Xu\**

*Abstract: Heterostructured metal—organic framework (MOF)-on-MOF thin films have the potential to cascade the various properties of different MOF layers in a sequence to produce functions that cannot be achieved by single MOF layers. An integration method that relies on van der Waals interactions, and which overcomes the lattice-matching limits of reported methods, has been developed. The method deposits molecular sieving Cu-TCPP (TCPP = 5,10,15,20-tetrakis-(4-carboxyphenyl)porphyrin) layers onto semiconductive Cu-HHTP (HHTP = 2,3,6,7,10,11-hexahydrotriphenylene) layers to obtain highly oriented MOF-on-MOF thin films. For the first time, the properties in different MOF layers were cascaded in sequence to synergistically produce an enhanced device function. Cu-TCPP-on-Cu-HHTP demonstrated excellent selectivity and the highest response to benzene of the reported recoverable chemiresistive sensing materials that are active at room temperature. This method allows integration of MOFs with cascading properties into advanced functional materials.*

$\mathbf{M}$etal–organic frameworks (MOFs) or porous coordination polymers (PCPs) are a kind of crystalline microporous materials constructed by periodic connection of inorganic and organic units.[1] Such materials have shown great potential in fields such as gas storage/separation, luminescence, magnetism, catalysis, and electronic/ionic conduction.[2] MOFs are typically prepared as crystalline powders. However, MOF thin films are favored for integration of such materials into diverse research fields.[3] In recent years, researchers have focused on the design and preparation of heterostructured multilayer MOF thin films.[4] The final target in this research

field is to build a cascade of MOF layers with different properties for advanced applications and, in so doing, to produce a complex function that cannot be achieved by a single MOF layer. Heterostructured MOF-on-MOF thin films have been prepared by stepwise liquid-phase epitaxial (LPE) growth of one MOF layer on another, which involves one-to-one coordination bonding at the interface.[5] Typically, the second MOF layer is required to match the structure or at least the lattice in the specific crystal surface of the first MOF layer. Unfortunately, MOFs with different properties generally possess distinct crystal unit cell parameters and even topological structure. Consequently, a method that can integrate different functional MOF layers independently of the lattice matching issue is extremely desirable but challenging. Numerous multilayer MOF thin films have been successfully prepared and structurally characterized, and their applications have been reported numerously.[5] Cascading the properties of different MOF layers, such as gas adsorption/separation and chemiresistive sensing properties, to realize an advanced device function has, however, not been reported to date.

Van der Waals (vdW) forces give access to a bond-free assembly method that can physically integrate different materials with weak vdW interactions.[6] Since it does not involve chemical bonding at the interface of two materials, vdW interactions are not limited to structurally matched materials. This method of integration has enjoyed great success in the preparation of the heterojunction of two-dimensional (2D) atomic crystals.[7] Herein, we report a convenient vdW integration method that enables assembly of two lattice-mismatched MOF layers, Cu-HHTP and Cu-TCPP (HHTP = 2,3,6,7,10,11-hexahydrotriphenylene and TCPP = 5,10,15,20-tetrakis(4-carboxyphenyl)porphyrin). With this method, MOF layers with rationally designed properties were assembled in sequence, as shown schematically in Figure 1, to produce an enhanced device function for the first time.

A complex device function was realized with a MOF-on-MOF thin film chemiresistive sensing material. MOFs have attracted growing interest as a new type of chemiresistive sensing material because of their tunable composition, ultra-high porosity, and the large amount of active sensing sites offered.[8] Interestingly, our research found that a semiconductive Cu-HHTP thin film has an obvious response to benzene at room temperature but it has an even higher response to polar gas molecule, such as $NH_3$. To demonstrate the advantages of MOF-on-MOF thin films, Cu-TCPP layers that can selectively suppress the penetration of $NH_3$ were integrated with Cu-HHTP using vdW forces. The molecular

[*] Dr. M. S. Yao,[+] J. W. Xiu,[+] Q. Q. Huang, W. H. Li, A. Q. Wu, L. A. Cao, W. H. Deng, Dr. G. E. Wang, Prof. G. Xu
State Key Laboratory of Structural Chemistry
Fujian Institute of Research on the Structure of Matter
Chinese Academy of Sciences (CAS)
155 Yangqiao Road West, Fuzhou, Fujian, 350002 (P. R. China)
E-mail: gxu@fjirsm.ac.cn

Q. Q. Huang, W. H. Li, L. A. Cao, W. H. Deng, Prof. G. Xu
University of Chinese Academy of Sciences (CAS)
Beijing 100039 (P. R. China)

Dr. W. W. Wu
School of Advanced Materials and Nanotechnology
Xidian University
Shaanxi, 710126 (P. R. China)

[+] These authors contributed equally to this work.

Supporting information and the ORCID identification number(s) for the author(s) of this article can be found under:
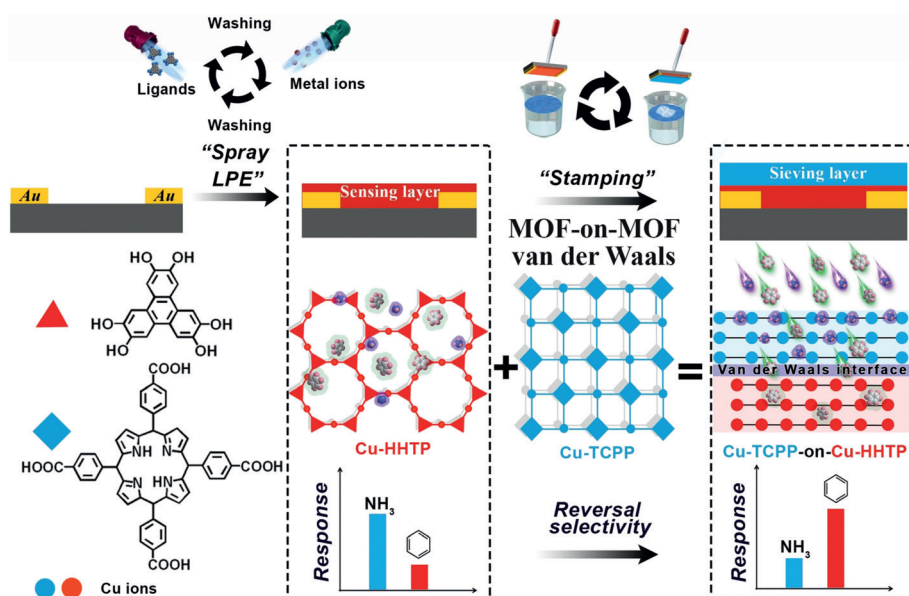https://doi.org/10.1002/anie.201907772.

**Figure 1.** Illustration of the preparation of MOF-on-MOF thin films by vdW integration and application of the films as highly selective benzene-sensing materials.

sieving layer and chemical sensing layer were easily integrated and the prepared Cu-TCPP-on-Cu-HHTP thin film demonstrated, to the best of our knowledge, the highest sensitivity and tunable selectivity to benzene at room temperature among all the reported recoverable chemiresistive materials.

Cu-HHTP has a honeycomb-like porous structure which is constructed by an AB stacking of extended hexagonal 2D π-conjugation layers to form honeycomb (hcb) topology (Figure 1; Supporting Information, Figure S1, Scheme S1a). Cu-HHTP thin films were prepared by a layer-by-layer spray LPE method on -OH functionalized substrates with pre-prepared Au interdigitated electrodes (Figure 1; Supporting Information).[8d] The thickness of Cu-HHTP was carefully controlled to an average of approximately 1.5 nm per cycle (Supporting Information, Figure S2).[8d] Subsequently, Cu-HHTP thin films were activated by successive immersions in *N,N*-dimethylformamide (DMF) and ethanol at room temperature (Supporting Information).

Cu-TCPP has square lattice (sql) topology, which differs from that of Cu-HHTP (Supporting Information, Figure S3). To solve the lattice mismatching issue, a "modular assembly" stamping method, which assembles MOF nanosheets into a highly oriented thin film, was employed to integrate Cu-TCPP and Cu-HHTP using vdW forces (Figure 1; Supporting Information, Scheme S1b).[9] Crystalline Cu-TCPP nanosheets of only a few-molecular layers thickness were prepared by a one-pot reaction of metal ions and H$_2$TCPP (Supporting Information, Figures S4 and S5). Subsequently, the nanosheets were dispersed

in ethanol to form a translucent suspension that was coated dropwise onto the surface of water in a beaker, forming a continuous layer (Figure 1). The Cu-TCPP layer was then transferred onto the surface of a Cu-HHTP layer by stamping. Upon repetition of these steps, the thickness of the Cu-TCPP layer increased with the number of cycles.

Cu-TCPP-xC-on-Cu-HHTP-yC thin films, where *x* (0–10) and *y* (10–50) are the growing cycles, have been successfully prepared (Figure 2; Supporting Information, Figures S2 and S6–S8). The scanning electron microscopy (SEM) and atomic force microscopy (AFM) images of the plane view of Cu-TCPP-xC-on-Cu-HHTP-20C (*x* = 0, 5, 10) are displayed in Figures 2a–f. Notably, Cu-TCPP-0C-on-Cu-HHTP-20C (that is, Cu-HHTP-20C) has a smooth and crack-free surface with a thickness of about 30 nm (Supporting Information, Figure S2) and roughness less than 2.5 nm. Transmission electron microscope (TEM) and selected area electron diffraction (SAED) images (Figure 2g; Supporting Information, Figure S9) of the Cu-HHTP thin film peeled away from the substrate demonstrate its pure crystal phase. The oriented growth of the Cu-HHTP thin film along the *c* axis is revealed
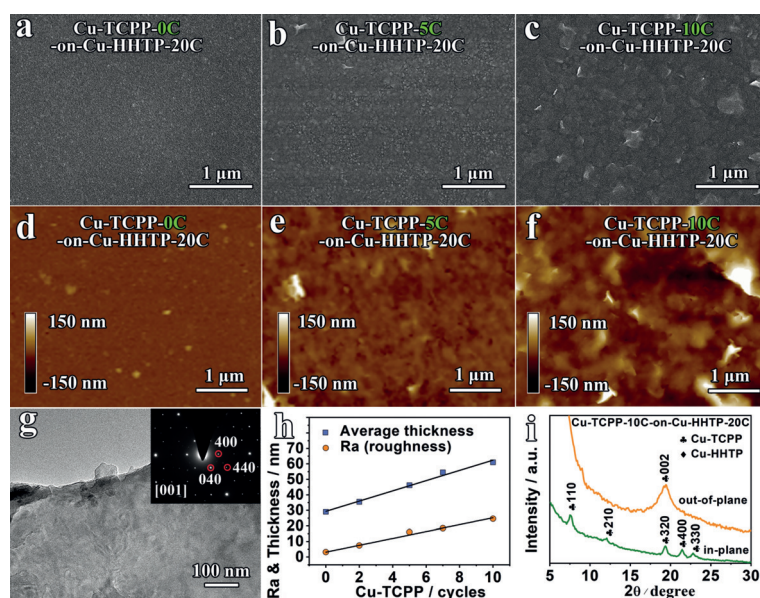


**Figure 2.** SEM and AFM images of a,d) Cu-TCPP-0C-on-Cu-HHTP-20C, b,e) Cu-TCPP-5C-on-Cu-HHTP-20C, and c,f) Cu-TCPP-10C-on-Cu-HHTP-20C. g) A TEM image of the Cu-HHTP-20C fragment (inset: SAED pattern). h) Cu-TCPP cycle-dependent roughness and thickness of Cu-TCPP-xC-on-Cu-HHTP-20C (*x* = 0, 2, 5, 7, and 10). i) In-plane and out-of-plane XRD patterns of Cu-TCPP-10C-on-Cu-HHTP-20C.

by an absence of (00l) the diffraction signal.[8d] When Cu-TCPP is stamped onto the Cu-HHTP layer, the thickness and roughness of the surface of Cu-TCPP-xC-on-Cu-HHTP-20C increased linearly to reach about 61 and 14.2 nm, respectively, when $x = 10$ (Figure 2h). The roughness of the film increased much more slowly in comparison to its thickness, indicating smooth growth of the Cu-TCPP layer on the Cu-HHTP layer. Figure 2i presents the in- and out-of-plane patterns of Cu-TCPP-10C-on-Cu-HHTP-20C, which were measured using grazing-incidence X-ray diffraction (XRD; Supporting Information). In the crystal structure of Cu-TCPP, the in-plane and out-of-plane peaks can be



**Figure 3.** Room temperature (RT) chemiresistive gas sensing properties. a) A response comparison of Cu-TCPP-0C-on-Cu-HHTP-yC ($x = 10$, 20, 30, 40, and 50). b) A comparison of responses and c) selectivity improvements for Cu-TCPP-xC-on-Cu-HHTP-20C ($x = 0$, 5, 10, 15, and 20). d) Concentration-dependent response–recovery curves. e) Normalized response–recovery time curves for Cu-TCPP-10C-on-Cu-HHTP-20C toward benzene gas. f) Linear log–log plots of response vs. concentration for Cu-TCPP-10C-on-Cu-HHTP-20C with respect to benzene gas and in comparison with reported benzene chemiresistive gas sensors working at RT. Key: multiwalled carbon nanotube (MWCNTs), 2,3,4,5,6-pentafluorophenylacetyl cellulose acetates (F5Ph-CA), polypyrrole (ppy), polyaniline (PANI), single-walled carbon nanotubes (SWCNTs), iron tetraphenyl porphyrin (FeTPP), tin oxide on graphene ($SnO_2$-G).

indexed as ($hk0$) and (00l), respectively, which indicates the oriented growth of a Cu-TCPP layer along the [001] direction (Supporting Information, Figure S3). As a consequence of the weak diffraction of Cu-HHTP in the bottom layer, an associated peak was not observed. TEM measurement of Cu-HHTP and XRD measurement of Cu-TCPP reveal that Cu-TCPP-10C-on-Cu-HHTP-20C is highly oriented and the one-dimensional channels in both MOFs are perpendicular to the substrate. After removal of part of the Cu-TCPP layer with scotch tape and manual removal of part of the Cu-HHTP layer with a pair of tweezers, the stage-like structure of Cu-TCPP-10C-on-Cu-HHTP-20C was clearly visible in an AFM image (Supporting Information, Figure S8).

Cu-TCPP, an electronic insulator, was selected as the gas molecular sieving layer because its 2D structure possesses abundant coordination-unsaturated Cu ions, which establish stronger interactions with $NH_3$ than with benzene (Figure 1). Cu-HHTP is a *p*-type semiconductive MOF material with a conductivity of $0.2 \, S\,cm^{-1}$ at room temperature.[8d,10] It was introduced as a gas-sensing signal-transducing layer. Therefore, cascading the properties of Cu-TCPP and Cu-HHTP in this way may result in a highly sensitive and selective gas-sensing material. The sensing performances of thin films with Cu-TCPP-xC-on-Cu-HHTP-yC were evaluated at room temperature by depositing them on a sapphire substrate that contains pre-prepared gold electrodes (Supporting Information).[8d,11]

Figure 3a presents the response of Cu-TCPP-0C-on-Cu-HHTP-yC (that is, Cu-HHTP-yC with different growing cycles) to 100 ppm $NH_3$ and benzene. It was found that, among all tested thin films, Cu-HHTP-20C has the required high response to both gases; thus, it was selected for further
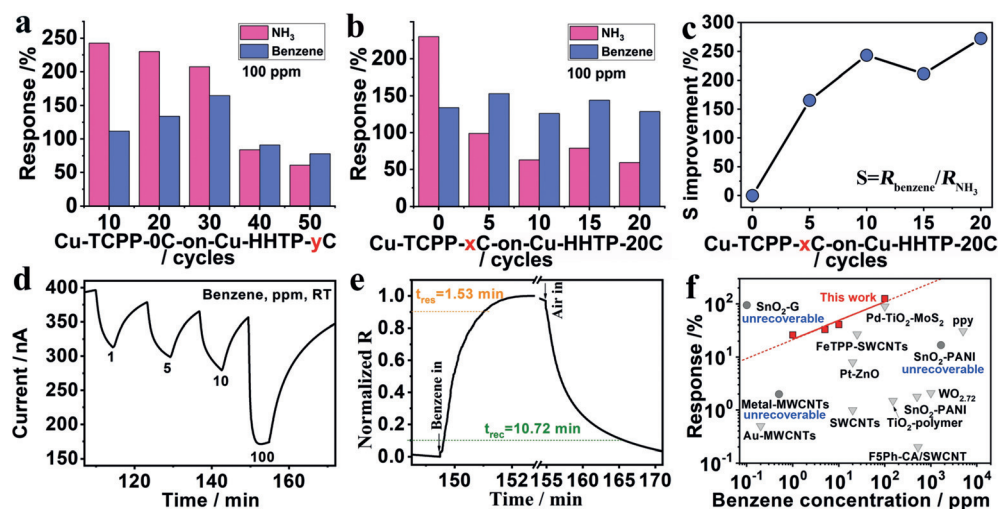
investigation as part of a composite with a Cu-TCPP coating. As shown in Figure 3b, after coating with a Cu-TCPP layer (5 cycles), Cu-HHTP-20C showed a remarkably decreased response to $NH_3$, from 230% to 94%, and a slightly enhanced response to benzene, from 134% to 153%. The selectivity ($S = R_{benzene}/R_{NH_3}$) of Cu-HHTP-20C toward benzene and $NH_3$ was reversed by depositing Cu-TCPP onto the Cu-HHTP-20C. The thicker Cu-TCPP layer further enhanced this reversed selectivity, which approaches saturation after 10 cycles (Figure 3c; Supporting Information, Figures S10 and S11). An improvement in S of up to about 250% was obtained by Cu-TCPP-10C-on-Cu-HHTP-20C compared with Cu-HHTP-20C. Cu-TCPP-10C-on-Cu-HHTP-20C also showed good response–recovery properties with respect to benzene at room temperature and its response increased with increments in the benzene concentration from 1 to 100 ppm (Figure 3d); its response and recovery times were estimated to be 1.53 and 10.72 min, respectively (Figure 3e). The theoretical limit of detection (LOD) to benzene was calculated to be 0.12 ppm from the linear log–log plots of responses vs. concentration by setting the response to 10% (Figure 3e). Notably, Cu-TCPP-10C-on-Cu-HHTP-20C exhibited the highest response toward benzene among the reported recoverable room temperature chemiresistors (Figure 3f).[12]

To investigate the sensing process in detail, Zn-TCPP (the isostructure of Cu-TCPP) was coated on the surface of Cu-HHTP using the same procedures (Supporting Information, Figure S12). Compared with the Cu-TCPP-10C layer, the Zn-TCPP-xC ($x = 5$, 10) layer caused little change to the sensitivity and selectivity of Cu-HHTP-20C toward to $NH_3$ and benzene (Figure 4a; Supporting Information, Figure S13). These results demonstrate the critical role of the
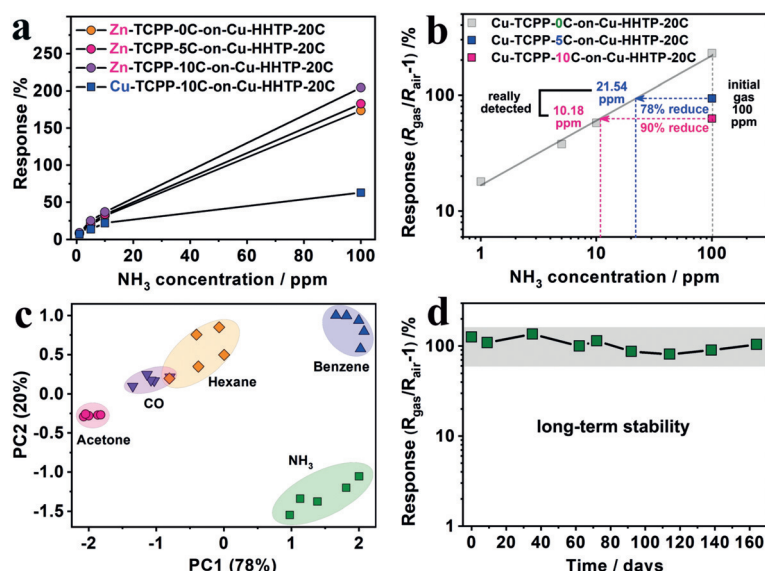
***Figure 4.*** a) Response–concentration plots for Zn-TCPP-xC-on-Cu-HHTP-20C ($y = 0$, 5, 10) and Cu-TCPP-10C-on-Cu-HHTP-20C toward $NH_3$ gas. b) Linear log–log plots of $NH_3$ response vs. concentration and estimated permeating concentrations. c) Principal component analysis of the MOF and MOF-on-MOF sensor array's responses to five typical biomarkers. d) The long-term stability of Cu-TCPP-10C-on-Cu-HHTP-20C toward 100 ppm benzene gas.

Cu-TCPP molecule sieving layer in reversing the selectivity of Cu-HHTP. Compared with $Zn^{2+}$, $Cu^{2+}$ has a stronger interaction with $NH_3$ at the axial positions of its octahedral coordination environment because of Jahn–Teller distortion, which blocks the permeation pathway of $NH_3$.[8e,13] Consequently, Cu-TCPP is better at suppressing the permeation of $NH_3$ over Zn-TCPP. Further data analysis revealed that Cu-TCPP-5C and Cu-TCPP-10C layers reduced permeation of 100 ppm $NH_3$ by approximately 78% and 90%, respectively (Figure 4b). After diffusing through the Cu-TCPP layer, analyte gases interact with Cu-HHTP. The subsequent charge transfers from gas molecules to *p*-type Cu-HHTP lead to a change in current.[8d,14,15] Under flowing dry air, the analyte gas is desorbed from Cu-HHTP, resulting in current recovery.

The selectivity of Cu-TCPP-on-Cu-HHTP was further investigated through discrimination of typical human breath biomarkers, such as $NH_3$, benzene, hexane, carbon monoxide, and acetone.[16] The responses of Cu-TCPP-0C-on-Cu-HHTP-20C and Cu-TCPP-20C-on-Cu-HHTP-yC ($y = 10, 20$) to these biomarkers were collected as sensors 1–3 and further analyzed by principal component analysis (Supporting Information, Tables S1 and S2). The principal components 1 and 2 (PC1 and PC2 account for 98% variance) for each subject are depicted in Figure 4c, which shows nearly non-overlapping and highly differentiated patterns for the five biomarkers. Cu-TCPP-10C-on-Cu-HHTP-20C also showed good long-term stability. After 5 months, about 80% of the original response value toward 100 ppm benzene was retained together with excellent selectivity (Figure 4d).

In summary, for the first time the different properties of MOF layers in heterostructured MOF-on-MOF thin films were cascaded to synergistically provide an enhanced device

function. The highly oriented MOF-on-MOF thin film was prepared by integrating the second MOF layer onto the first MOF layer using vdW forces. This method is convenient and avoids the need to consider the lattice matching conditions required by earlier methods for the growth of MOF-on-MOF thin films. Benefiting from this method, a molecular sieving MOF layer, Cu-TCPP, was integrated onto a chemiresistive sensing MOF layer, Cu-HHTP, with controlled thickness. The cascading properties of Cu-TCPP-on-Cu-HHTP realized the highest response to benzene of all reported room temperature chemiresistive sensing materials, and reversed the selectivity of Cu-HHTP toward benzene and the strongly interfering molecule, $NH_3$. Furthermore, through principal component analysis of the data collected with Cu-TCPP-xC-on-Cu-HHTP-20C, five typical human breath biomarkers were clearly detected and distinguished. This work enriches the preparative chemistry for heterostructure MOF-on-MOF thin films. The ordered integration of various MOF properties achieved in this work introduces a new strategy by which the made-to-order functions of MOF materials may be realized in advanced device applications.

## Conflict of interest

The authors declare no conflict of interest.

[1] a) H. Furukawa, K. E. Cordova, M. O'Keeffe, O. M. Yaghi, *Science* **2013**, *341*, 1230444; b) H. Deng, C. J. Doonan, H. Furukawa, R. B. Ferreira, J. Towne, C. B. Knobler, B. Wang, O. M. Yaghi, *Science* **2010**, *327*, 846–850; c) P.-Q. Liao, W.-X. Zhang, J.-P. Zhang, X.-M. Chen, *Nat. Commun.* **2015**, *6*, 8697; d) H.-C. J. Zhou, S. Kitagawa, *Chem. Soc. Rev.* **2014**, *43*, 5415–5418; e) K. Sumida, D. L. Rogow, J. A. Mason, T. M. McDonald, E. D. Bloch, Z. R. Herm, T.-H. Bae, J. R. Long, *Chem. Rev.* **2012**,

14918    www.angewandte.org

© 2019 Wiley-VCH Verlag GmbH & Co. KGaA, Weinheim

*Angew. Chem. Int. Ed.* **2019**, *58*, 14915–14919

*112*, 724–781; f) Q.-G. Zhai, X. Bu, X. Zhao, D.-S. Li, P. Feng, *Acc. Chem. Res.* **2017**, *50*, 407–417; g) Q. Yang, D. Liu, C. Zhong, J.-R. Li, *Chem. Rev.* **2013**, *113*, 8261–8323; h) T. Islamoglu, S. Goswami, Z. Li, A. J. Howarth, O. K. Farha, J. T. Hupp, *Acc. Chem. Res.* **2017**, *50*, 805–813; i) X. Liu, B. Tang, J. Long, W. Zhang, X. Liu, Z. Mirza, *Sci. Bull.* **2018**, *63*, 502–524.

[2] a) M. Ding, R. W. Flaig, H.-L. Jiang, O. M. Yaghi, *Chem. Soc. Rev.* **2019**, *48*, 2783–2828; b) L. Li, R.-B. Lin, R. Krishna, H. Li, S. Xiang, H. Wu, J. Li, W. Zhou, B. Chen, *Science* **2018**, *362*, 443–446; c) V. Stavila, A. Talin, M. Allendorf, *Chem. Soc. Rev.* **2014**, *43*, 5994–6010; d) P. Ramaswamy, N. E. Wong, G. K. Shimizu, *Chem. Soc. Rev.* **2014**, *43*, 5913–5932; e) Q. Xu, H. Kitagawa, *Adv. Mater.* **2018**, *30*, 1803613; f) C. Gu, N. Hosono, J.-J. Zheng, Y. Sato, S. Kusaka, S. Sakaki, S. Kitagawa, *Science* **2019**, *363*, 387–391.

[3] a) D. Zacher, O. Shekhah, C. Wöll, R. A. Fischer, *Chem. Soc. Rev.* **2009**, *38*, 1418–1429; b) K. Ono, M. Ishizaki, K. Kanaizuka, T. Togashi, T. Yamada, H. Kitagawa, M. Kurihara, *Angew. Chem. Int. Ed.* **2017**, *56*, 5531–5535; *Angew. Chem.* **2017**, *129*, 5623–5627; c) E. Virmani, J. M. Rotter, A. Mähringer, T. Von Zons, A. Godt, T. Bein, S. Wuttke, D. D. Medina, *J. Am. Chem. Soc.* **2018**, *140*, 4812–4819; d) Z. G. Gu, D. J. Li, C. Zheng, Y. Kang, C. Wöll, J. Zhang, *Angew. Chem. Int. Ed.* **2017**, *56*, 6853–6858; *Angew. Chem.* **2017**, *129*, 6957–6962; e) I. Stassen, N. Burtch, A. Talin, P. Falcaro, M. Allendorf, R. Ameloot, *Chem. Soc. Rev.* **2017**, *46*, 3185–3241; f) O. Shekhah, H. Wang, S. Kowarik, F. Schreiber, M. Paulus, M. Tolan, C. Sternemann, F. Evers, D. Zacher, R. A. Fischer, C. Wöll, *J. Am. Chem. Soc.* **2007**, *129*, 15118–15119.

[4] a) K. Ikigaki, K. Okada, Y. Tokudome, T. Toyao, P. Falcaro, C. J. Doonan, M. Takahashi, *Angew. Chem. Int. Ed.* **2019**, *58*, 6886–6890; b) B. Liu, M. Ma, D. Zacher, A. Bétard, K. Yusenko, N. Metzler-Nolte, C. Wöll, R. A. Fischer, *J. Am. Chem. Soc.* **2011**, *133*, 1734–1737.

[5] a) B. Liu, M. Tu, D. Zacher, R. A. Fischer, *Adv. Funct. Mater.* **2013**, *23*, 3790–3798; b) V. Chernikova, O. Shekhah, I. Spanopoulos, P. N. Trikalitis, M. Eddaoudi, *Chem. Commun.* **2017**, *53*, 6191–6194; c) O. Shekhah, K. Hirai, H. Wang, H. Uehara, M. Kondo, S. Diring, D. Zacher, R. A. Fischer, O. Sakata, S. Kitagawa, S. Furukawa, C. Wöll, *Dalton Trans.* **2011**, *40*, 4954–4958; d) Z. Wang, J. Liu, B. Lukose, Z. Gu, P. G. Weidler, H. Gliemann, T. Heine, C. Wöll, *Nano Lett.* **2014**, *14*, 1526–1529.

[6] Y. Liu, Y. Huang, X. Duan, *Nature* **2019**, *567*, 323.

[7] a) L. Ju, L. Wang, T. Cao, T. Taniguchi, K. Watanabe, S. G. Louie, F. Rana, J. Park, J. Hone, F. Wang, *Science* **2017**, *358*, 907–910; b) W. Xu, W. Liu, J. F. Schmidt, W. Zhao, X. Lu, T. Raab, C. Diederichs, W. Gao, D. V. Seletskiy, Q. Xiong, *Nature* **2017**, *541*, 62–67; c) K. Kang, K.-H. Lee, Y. Han, H. Gao, S. Xie, D. A. Muller, J. Park, *Nature* **2017**, *550*, 229–233; d) Z. Zhang, P. Chen, X. Duan, K. Zang, J. Luo, X. Duan, *Science* **2017**, *357*, 788–792.

[8] a) W.-T. Koo, J.-S. Jang, I.-D. Kim, *Chem* **2019**, *5*, 1938–1963; b) Z. Meng, R. M. Stolz, L. Mendecki, K. A. Mirica, *Chem. Rev.* **2019**, *119*, 478–598; c) M. Ko, L. Mendecki, K. A. Mirica, *Chem. Commun.* **2018**, *54*, 7873–7891; d) M.-S. Yao, X.-J. Lv, Z.-H. Fu, W.-H. Li, W.-H. Deng, G.-D. Wu, G. Xu, *Angew. Chem. Int. Ed.* **2017**, *56*, 16510–16514; *Angew. Chem.* **2017**, *129*, 16737–16741; e) M. G. Campbell, D. Sheberla, S. F. Liu, T. M. Swager, M. Dincă, *Angew. Chem. Int. Ed.* **2015**, *54*, 4349–4352; *Angew. Chem.* **2015**, *127*, 4423–4426; f) Z. Meng, A. Aykanat, K. A. Mirica, *J. Am. Chem. Soc.* **2019**, *141*, 2046–2053; g) M. L. Aubrey, M. T. Kapelewski, J. F. Melville, J. Oktawiec, D. Presti, L. Gagliardi, J. R. Long, *J. Am. Chem. Soc.* **2019**, *141*, 5005–5013.

[9] a) G. Xu, T. Yamada, K. Otsubo, S. Sakaida, H. Kitagawa, *J. Am. Chem. Soc.* **2012**, *134*, 16524–16527; b) G. Xu, K. Otsubo, T. Yamada, S. Sakaida, H. Kitagawa, *J. Am. Chem. Soc.* **2013**, *135*, 7438–7441.

[10] a) M. G. Campbell, S. F. Liu, T. M. Swager, M. Dincă, *J. Am. Chem. Soc.* **2015**, *137*, 13780–13783; b) W. H. Li, K. Ding, H. R. Tian, M. S. Yao, B. Nath, W. H. Deng, Y. Wang, G. Xu, *Adv. Funct. Mater.* **2017**, *27*, 1702067.

[11] M. S. Yao, W. X. Tang, G. E. Wang, B. Nath, G. Xu, *Adv. Mater.* **2016**, *28*, 5229–5234.

[12] a) J. Li, Y. Lu, Q. Ye, M. Cinke, J. Han, M. Meyyappan, *Nano Lett.* **2003**, *3*, 929–933; b) R. Leghrib, A. Felten, F. Demoisson, F. Reniers, J.-J. Pireaux, E. Llobet, *Carbon* **2010**, *48*, 3477–3484; c) M. Mabrook, P. Hawkins, *Sens. Actuators B* **2001**, *75*, 197–202; d) C. Murugan, E. Subramanian, D. P. Padiyan, *Synth. Met.* **2014**, *192*, 106–112; e) A. Katoch, S.-W. Choi, G.-J. Sun, S. S. Kim, *J. Nanosci. Nanotechnol.* **2013**, *13*, 7097–7099; f) P. Clément, S. Korom, C. Struzzi, E. J. Parra, C. Bittencourt, P. Ballester, E. Llobet, *Adv. Funct. Mater.* **2015**, *25*, 4011–4020; g) D. Zhang, C. Jiang, X. Zhou, *Talanta* **2018**, *182*, 324–332; h) M. F. Mabrook, C. Pearson, M. C. Petty, *Sens. Actuators B* **2006**, *115*, 547–551; i) J. Im, E. Sterner, T. Swager, *Sensors* **2016**, *16*, 183; j) Y. S. Kim, *Sens. Actuators B* **2009**, *137*, 297–304; k) F.-L. Meng, H.-H. Li, L.-T. Kong, J.-Y. Liu, Z. Jin, W. Li, Y. Jia, J.-H. Liu, X.-J. Huang, *Anal. Chim. Acta* **2012**, *736*, 100–107.

[13] a) T. Yu, T. Hao, D. Fan, J. Wang, M. Shen, W. Li, *J. Phys. Chem. C* **2014**, *118*, 6565–6575; b) L. Ma, Y. Cheng, G. Cavataio, R. W. McCabe, L. Fu, J. Li, *Appl. Catal. B* **2014**, *156*, 428–437.

[14] H. Liu, X. Li, L. Chen, X. Wang, H. Pan, X. Zhang, M. Zhao, *J. Phys. Chem. C* **2016**, *120*, 3846–3852.

[15] S.-J. Choi, I.-D. Kim, *Electron. Mater. Lett.* **2018**, *14*, 221–260.

[16] a) H. Haick, Y. Y. Broza, P. Mochalski, V. Ruzsanyi, A. Amann, *Chem. Soc. Rev.* **2014**, *43*, 1423–1449; b) R. Yazbeck, S. E. Jaenisch, D. I. Watson, *World J. Gastroenterol.* **2016**, *22*, 10077.